

Spectro-temporal dynamics of Kerr combs with parametric seeding

Guoping Lin,^{1,*} Romain Martinenghi,¹ Souleymane Diallo,¹ Khaldoun Saleh,¹
Aurélien Coillet,^{1,2} and Yanne K. Chembo¹

¹FEMTO-ST Institute [CNRS UMR6174], Optics Department, 15B Avenue des Montboucons,
25030 Besançon cedex, France

²NIST, Boulder, Colorado 80305, USA

*Corresponding author: guoping.lin@femto-st.fr

Received 16 December 2014; revised 9 February 2015; accepted 17 February 2015;
posted 17 February 2015 (Doc. ID 230895); published 18 March 2015

We report a joint theoretical and experimental investigation of the parametric seeding of a primary Kerr optical frequency comb. Electro-optic modulation sidebands matching multiple free-spectral ranges of an ultrahigh- Q millimeter-size magnesium fluoride disk resonator are used as seed signals. These seed signals interact through four-wave mixing with the spectral components of a stable primary comb and give rise to complex spectro-temporal patterns. We show that the new frequency combs feature multiscale frequency spacing, with major frequency gaps in the order of a few hundred gigahertz, and minor frequency spacing in the order of a few tens of gigahertz. The experimental results are in agreement with numerical simulations using the Lugiato-Lefever equation. We expect such versatile and coherent optical frequency combs to have potential applications in optical communications systems where frequency management assigns predefined spectral windows at the emitter stage. © 2015 Optical Society of America

OCIS codes: (140.4780) Optical resonators; (190.4410) Nonlinear optics, parametric processes; (190.4380) Nonlinear optics, four-wave mixing.

<http://dx.doi.org/10.1364/AO.54.002407>

1. Introduction

In recent years, multifrequency laser sources with strictly equidistant spacing, known as frequency combs, have been attracting great interest in the fields of metrology, spectroscopy, sensing, and coherent optical communications. Traditional comb sources are based on mode-locked lasers. An alternate approach for producing such optical frequency combs has been reported by using parametric four-wave mixing (FWM) in ultrahigh quality (Q) factor whispering gallery mode (WGM) microresonators [1]. These combs are thus generally referred to as Kerr combs.

WGM resonators are interesting platforms for various applications based on nonlinear optical processes, as they can simultaneously feature ultrahigh Q factors and small mode volumes [2]. The resulting long photon lifetime and tight confinement facilitate interaction between the host materials and the intracavity optical fields. Demonstration of ultrahigh- Q WGM resonators from highly transparent crystals [3] has enabled efficient nonlinear frequency conversion into the ultraviolet (UV) [4,5] and mid-infrared light (MIR) [6] regimes. Beside crystalline WGM resonator-based Kerr frequency combs [6–9], chip-scale platforms using high- Q racetrack resonators have also shown the capabilities of Kerr frequency comb generation [10–14].

More recently, Kerr frequency combs used as multiwavelength carriers in coherent terabit communication were demonstrated [9]. This has sparked

interest in the field of optical communication as Kerr combs provide a compact, coherent, and energy-efficient multiwavelength source. However, the formation of Kerr combs can also involve many stages and could lead to nonequidistant combs with multiple radio-frequency (RF) beatnotes that are not equal to single or multiple free-spectral ranges (FSRs) [12,13,15]. The most robust and coherent comb generally arises through modulational instability (MI), which asymptotically leads to a roll pattern (or azimuthal Turing pattern) in the spatial domain, and to the so-called primary combs in the spectral domain [16–18].

A very important pioneering work was presented in [19], where parametric seeding was used to control the fully developed Kerr combs. In this article, we focus on the seeding dynamics in the particular regime of stable primary Kerr combs. This seeding procedure can provide frequency combs in predefined windows as shown in Fig. 1, compared with traditional combs generated by electro-optic modulation or mode locking. A millimeter-size ultrahigh- Q magnesium fluoride (MgF_2) disk resonator has been used in our experimental work. EOM sidebands matching multiple cavity FSRs are used as seeds. Numerical simulations based on a normalized Lugiato–Lefever equation are carried out and are in agreement with the experimental results.

2. Theoretical Model

Kerr optical frequency combs in ultrahigh- Q resonators are particularly interesting owing to their simplicity, compact size, and high efficiency. Their core element is a nonlinear bulk cavity in which cascaded FWM originates from the interplay between the Kerr nonlinearity of the host material and the dispersion. To simulate the comb formation, we use a normalized Lugiato–Lefever equation with periodic boundary conditions [18,20,21]:

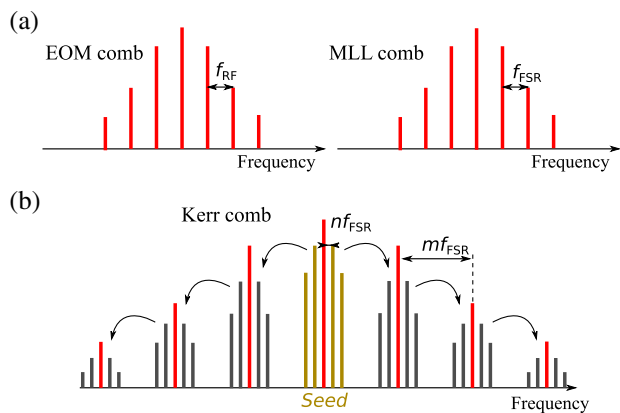


Fig. 1. Sketch of multifrequency comb sources. (a) Left, electro-optic modulation (EOM) based combs; f_{RF} , RF modulation frequency; right, mode-locked laser (MLL) based combs; f_{FSR} , cavity FSR. (b) Proposal for a dual spacing frequency comb using parametric seeded Kerr combs in monolithic resonators. Red, primary comb; gold, seed signals; gray, seeded Kerr combs.

$$\frac{\partial \psi}{\partial \tau} = -(1 + i\alpha)\psi + i|\psi|^2\psi - i\frac{\beta}{2}\frac{\partial^2 \psi}{\partial \theta^2} + F, \quad (1)$$

where ψ is the total intracavity field in the moving frame, $\tau = \Delta\omega_{\text{tot}}t/2 = t/(2\tau_{\text{photon}})$ is the dimensionless time with $\Delta\omega_{\text{tot}}$ being the mode linewidth and τ_{photon} being the photon lifetime, and θ from $-\pi$ to π is the azimuthal angle along the circumference of the disk. The dimensionless parameters in Eq. (1) are α , β , and F , where $\alpha = -2(\omega_L - \omega_R)/\Delta\omega_{\text{tot}}$ is the normalized frequency detuning between the continuous-wave (cw) laser frequency ω_L and the resonance position ω_R , $\beta = -2\zeta_2/\Delta\omega_{\text{tot}}$ is the dispersion, with ζ_2 being the second-order Taylor coefficient of the expansion, and F^2 is proportional to the external pump power. The intracavity power and the pump power at the input (in watts) can be recovered from their normalized counterparts as $|\mathcal{E}|^2 = [\Delta\omega_{\text{tot}}/2\gamma v_g]|\psi|^2$ and $P = [T_{\text{FSR}}\Delta\omega_{\text{tot}}^3/8\gamma v_g\Delta\omega_{\text{ext}}]F^2$, where v_g is the group velocity dispersion, $\Delta\omega_{\text{tot,ext}}$ are the total (loaded) and extrinsic (coupling) quality factors, γ is the Kerr-nonlinearity coefficient, and T_{FSR} is the intracavity round-trip time.

Numerical simulations are carried out using the split-step Fourier algorithm. The parametric seed signals are multiple ($n\times$) FSRs away from the pump signal. The corresponding power is very low with respect to the pump; therefore, one can use $F = F_0 + F_1 \sin(n\theta)$ to simulate the pump and seed signals. It should also be noted that the seed signals are inserted after the Turing pattern is obtained. Additionally, the output field of the coupler is treated as the sum of the pump field F_0 and a portion of the intracavity field ψ [22].

The primary combs arise after MI, and they correspond to a (phase-locked) primary comb in the spectral domain [16,17]. Figure 2 shows an illustration of the primary comb formation. The resonant cw pump laser first leads to MI gain, which is related to the three parameters α , β , and F [18]. Parametric FWM then generates the first two sidebands. They correspond to the WGMs located in the peak gain regime and are multiple FSRs away. Subsequent cascaded FWM processes create a stable primary comb spectrum. Although both stable soliton combs and self-phase-locked combs have recently been demonstrated [8,23], the primary comb is still the easiest and most robust phase-locked regime that can be accessed experimentally.

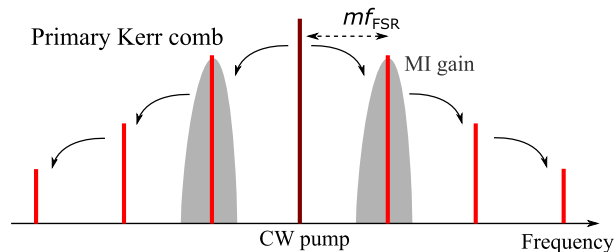


Fig. 2. Illustration of the onset of the primary Kerr comb. Gray zone highlights the MI gain.

The gain profile in the primary comb regime can be calculated by linearizing the Lugiato–Lefever equation close to the cw solution:

$$\frac{\partial}{\partial \tau} \delta \psi = -(1 + i\alpha) \delta \psi + 2i|\psi_e|^2 \delta \psi + i\psi_e^2 \delta \psi^* - i \frac{\beta}{2} \frac{\partial^2}{\partial \theta^2} \delta \psi. \quad (2)$$

Here, $\delta \psi$ is a perturbation of the steady-state equilibrium ψ_e . An expansion of this perturbation $\delta \psi$ along the different WGMs of the resonator leads to the calculation of the parametric gain for a given mode number l [18]:

$$\Gamma(l) = \Re \left\{ -1 + \sqrt{\rho^2 - \left[\alpha - 2\rho - \frac{1}{2}\beta l^2 \right]^2} \right\}, \quad (3)$$

where $\rho = |\psi_e|^2$. Figure 3 shows the shape of this parametric gain for two sets of parameters. The modes for which the gain is greater than zero can experience growth, which will ultimately lead to the generation of a Turing pattern. As can be seen in Fig. 3, several modes satisfy this condition and can therefore be excited.

3. Experimental Setup

The monolithic MgF₂ resonator used in this experiment is fabricated using a commercially available preformed disk with a radius of 6 mm and a thickness of 1 mm. The disk was then submitted to a sequence of grinding and polishing processes, until the root mean square surface roughness of the rim reached only a few nanometers [24]. The resulting MgF₂ resonator supports an intrinsic Q factor of 10⁹ at the wavelength of 1550 nm.

The experimental setup for frequency comb generation is illustrated schematically in Fig. 4. A tunable cw diode laser featuring a few kilohertz spectral linewidth is used as the single-frequency pump source. A fiber polarization controller is inserted for optimizing the WGM excitation. The seed signals are then provided using a phase electro-optic modulator (EOM) with a tunable RF synthesizer. The laser power is further amplified using an erbium-doped

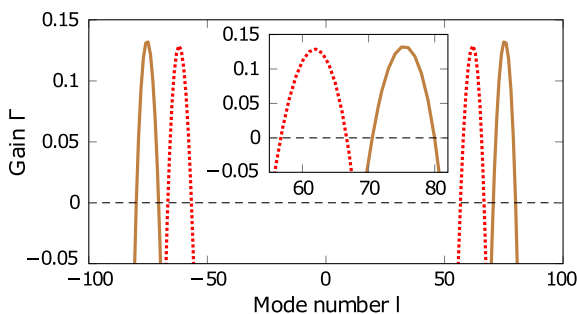


Fig. 3. Parametric gain as a function of the mode number. The parameters used are those of Figs. 5 and 6: $\alpha = -1$, $\beta = -0.0017$, $F = 2.5$ for the dotted red curve and $\alpha = -2$, $\beta = -0.0015$, $F = 3.5$ for the solid brown curve.

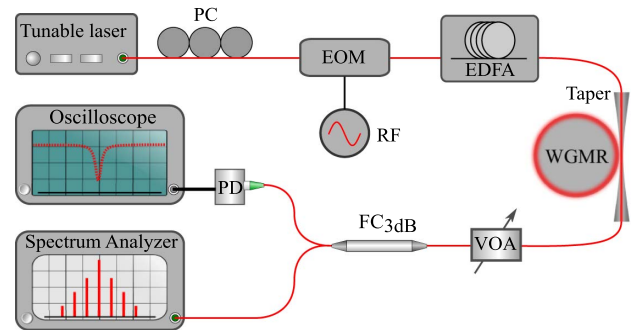


Fig. 4. Schematic view of the experimental setup. PC, polarization controller; EOM, phase electro-optic modulator; RF, radio-frequency synthesizer; EDFA, erbium-doped fiber amplifier; WGMR, MgF₂ whispering gallery mode resonator; VOA, variable optical attenuator; FC_{3dB}, 3 dB 1 × 2 fiber coupler; PD, InGaAs photodetector; OSA, optical spectrum analyzer.

fiber amplifier (EDFA). The final pump power can reach a few hundred milliwatts. In this experiment, we focus on the investigation and demonstration of the seeded comb signals in the stable primary comb or Turing pattern regime [22]. The excitation of WGMs in the MgF₂ disk resonator is accomplished through evanescent wave coupling, using a tapered single-mode fiber for both input and output coupling [25]. The output signal passes through a variable fiber attenuator, connected to a 3 dB, 1 × 2 fiber coupler. The split signals are then separately monitored using a photodetector (PD) and a high-resolution optical spectrum analyzer (OSA, APEX2440B).

4. Results and Discussion

Ultrahigh- Q WGM resonators usually feature rich transversely distributed modes within one FSR in either the radial or polar direction [26]. The dispersion parameter shown in Eq. (1) is determined by the combination of material dispersion and cavity dispersion that relies on mode properties. A tunable cw laser source being able to cover one full FSR range is thus required in the detailed exploration of WGM-based Kerr frequency combs. Meanwhile, as shown in Eq. (1), the formation of Kerr optical frequency combs also relies strongly on the frequency detuning parameter α . Therefore, the pump laser frequency should be fixed relatively to the cavity resonance position for stable operation. This can be achieved using an active locking method such as the Pound–Drever–Hall method or a passive method. Concerning the latter, one can use either self-injection locking [27], which can be very compact, or self-thermal locking, which has also been demonstrated for microlaser characterizations [28]. Since self-thermal locking is an easy and simple method, it is utilized throughout our experiments. Considering that MgF₂ material has positive thermo-optic and thermal expansion coefficients, the pump laser frequency is changed from the shorter wavelength side toward the WGM for the self-thermal locking.

Primary combs usually feature multiple-FSR spacing in the frequency domain, up to several hundred

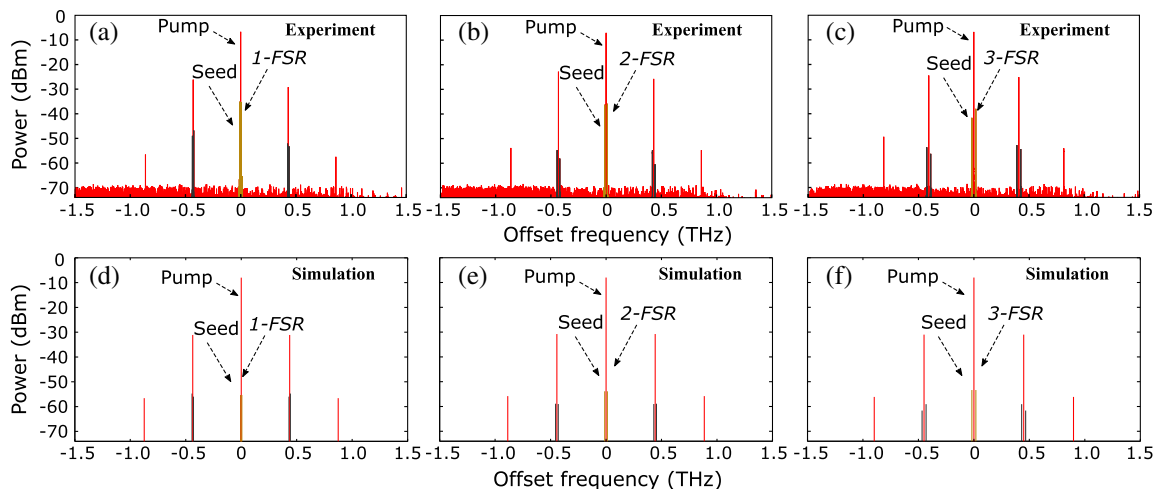


Fig. 5. Comparison of experimental parametric seeded comb spectra and numerical simulation results. The primary Kerr comb spacing m -FSR: 73-FSR. (a)–(c) Experimental results. (d)–(f) Numerical simulations, with $\alpha = -2$, $\beta = -0.0015$, and $F_0 = 3.5$. The seed signal spacing n -FSR and F_1 are 1-FSR, 2-FSR, and 3-FSR and 0.03, 0.04, and 0.05 from left to right, respectively.

FSRs. Depending on the FSR value, the primary comb spacing can be larger than 50 nm or 6 THz for an on-chip waveguide resonator [11]. The resonator we have investigated has a diameter slightly smaller than 12 mm. We first obtained a primary Kerr comb with spacing of 73-FSR through self-thermal locked pumping. To get the single FSR value, we temporarily changed the pump detuning to observe the subcomb generation with single FSR spacing. The FSR value was then read out from the RF beatnote spectrum obtained using a fast PD and an electrical spectrum analyzer. Since the detuning change also results in the change of the resonator temperature due to different coupled pump power, the FSR value at the primary comb stage slightly differs from the measured one. It should be noted that the sideband spectroscopy technique can also be used to measure the FSR values [29]. Subsequently, we applied 1-FSR, 2-FSR, and 3-FSR (5.9066, 11.8128, and 17.7190 GHz) RF signals to drive the EOM for generating sidebands as the seed and pump signals. The corresponding experimental spectra obtained in the OSA are presented in Figs. 5(a)–5(c), respectively. It should be noted that the seeded Kerr comb signals (in gray) disappear as soon as the seeds (in gold) are switched off. Because the parametric gain is centered around the primary comb components (signal/idler pairs), the closest seeds relative to these frequency components will have the largest gain, through the FWM process between the seeds and the primary combs. This phenomenon is observed both experimentally and theoretically. Figures 5(d)–5(f) show the numerical simulations, which are in agreement with the experimental results within the accuracy range of our measurement devices. It should also be noted that the tuning step of our RF synthesizer (100 kHz) is comparable to the resonance linewidth, and forbids the fine tuning that could lead to even better matching.

Figure 6(a) presents the experimental spectrum on 1-FSR sideband seeded Kerr combs when another

WGM is pumped. The primary comb spacing here is 62-FSR with a single FSR equal to 5.9013 GHz. Here we further increase the power of the seed signals by increasing the RF power that drives the EOM. It results in many pairs of equidistant seed components. The seeds then generate new frequency components that are scattered around the primary comb through FWM. As a result, they are strictly equidistant to the RF signal that is equal to one FSR. The corresponding simulation is given in Fig. 6(b). The spatio-temporal description of this seeded comb is shown in Fig. 7(a). The Turing pattern corresponding to a series of 62 equidistant pulses is heavily distorted by the modulation, with the height of each

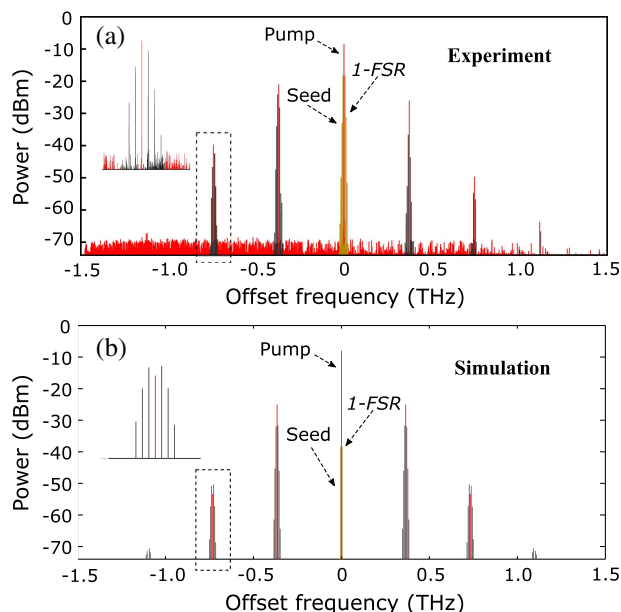


Fig. 6. Experimental result of a primary comb with 62-FSR spacing and cascaded parametric seed signals with 1-FSR spacing. (b) Corresponding numerical simulations: $\alpha = -1$, $\beta = -0.0017$, and $F = 2.5 + 0.12 \sin(\theta) + 0.05 \sin(2\theta)$.

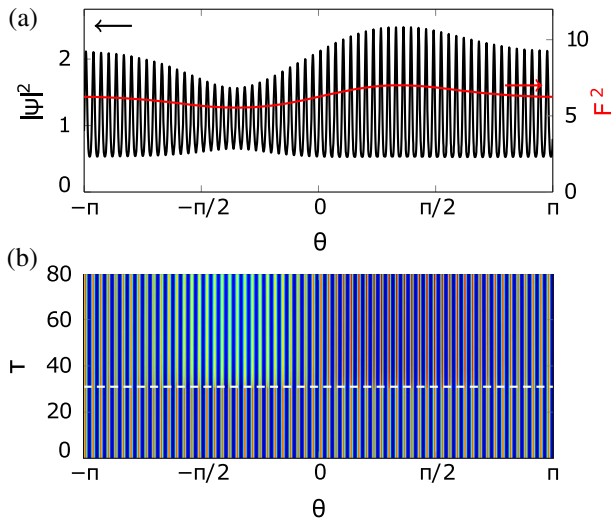


Fig. 7. Turing pattern of Fig. 6 in the spatio-temporal domain. The stationary state of the modulated pattern is represented in (a), and a strong variation in the pulses' height is observed. The corresponding excitation F^2 is shown in red on the same graph. The time evolution of the pattern when the modulation is switched on is presented in (b), the dashed line indicating the beginning of the modulation.

pulse strongly changing depending on the position of the pulse in the cavity. The corresponding excitation power F^2 is shown in red (right ordinate axis). As expected, the pulses of maximum amplitude are located where the pump is the strongest. Figure 7(b) focuses on the time evolution of the intracavity optical power when the modulation is abruptly switched on, and shows that the system quickly evolves from an unperturbed Turing pattern to its stationary states, within few tens of photon lifetimes.

In general, asymmetric Kerr combs can be observed due to the dispersion profile change resulting from mode crossing in such resonators [30–32]. It is noteworthy that the problem of multichromatic pumping has been studied in many different configurations [19,33,34], and has enabled one to foreshadow many potential applications. Here, we have specifically focused our investigations on a configuration in which the parametric seeding allows for the generation of a dual-scale frequency comb. More complex seeding procedures can yield an even higher level of versatility for the optical frequency comb.

5. Conclusion

In conclusion, we have reported the generation of multifrequency comb sources in a monolithic crystalline disk resonator, using a single laser and its parametric sidebands as the pump and seed signals. Numerical simulations based on a normalized Lugiato–Lefever equation are carried out to investigate this method. New equidistant comb components are generated through FWM processes between the stable primary combs and the EOM combs. We expect that the resulting optical frequency combs could serve as multifrequency carriers in coherent optical

communications systems, or in other photonic systems in which the generation of versatile multiwavelength optical signals is of particular interest.

The authors acknowledge financial support from the European Research Council (ERC) through the projects NextPhase and Versyt. They also acknowledge financial support from the *Centre National d'Etudes Spatiales* (CNES) through the project SHYRO, from the *Région de Franche-Comté*, and from the Labex ACTION.

References

1. P. DelHaye, A. Schliesser, O. Arcizet, T. Wilken, R. Holzwarth, and T. Kippenberg, "Optical frequency comb generation from a monolithic microresonator," *Nature* **450**, 1214–1217 (2007).
2. K. J. Vahala, "Optical microcavities," *Nature* **424**, 839–846 (2003).
3. V. S. Ilchenko, A. A. Savchenkov, A. B. Matsko, and L. Maleki, "Nonlinear optics and crystalline whispering gallery mode cavities," *Phys. Rev. Lett.* **92**, 043903 (2004).
4. G. Lin, J. U. Fürst, D. V. Strekalov, and N. Yu, "Wide-range cyclic phase matching and second harmonic generation in whispering gallery resonators," *Appl. Phys. Lett.* **103**, 181107 (2013).
5. G. Lin and N. Yu, "Continuous tuning of double resonance-enhanced second harmonic generation in a dispersive dielectric resonator," *Opt. Express* **22**, 557–562 (2014).
6. C. Wang, T. Herr, P. DelHaye, A. Schliesser, J. Hofer, R. Holzwarth, T. Hänsch, N. Picqué, and T. Kippenberg, "Mid-infrared optical frequency combs at 2.5 μm based on crystalline microresonators," *Nat. Commun.* **4**, 1345 (2013).
7. A. A. Savchenkov, A. B. Matsko, V. S. Ilchenko, I. Solomatine, D. Seidel, and L. Maleki, "Tunable optical frequency comb with a crystalline whispering gallery mode resonator," *Phys. Rev. Lett.* **101**, 093902 (2008).
8. T. Herr, V. Brasch, J. Jost, C. Wang, N. Kondratiev, M. Gorodetsky, and T. Kippenberg, "Temporal solitons in optical microresonators," *Nat. Photonics* **8**, 145–152 (2014).
9. J. Pfeifle, V. Brasch, M. Lauerer, Y. Yu, D. Wegner, T. Herr, K. Hartinger, P. Schindler, K. Li, D. Hillerkuss, R. Schmogrow, C. Weimann, R. Holzwarth, W. Freude, J. Leuthold, T. J. Kippenberg, and C. Koos, "Coherent terabit communications with microresonator Kerr frequency combs," *Nat. Photonics* **8**, 375–380 (2014).
10. J. S. Levy, A. Gondarenko, M. A. Foster, A. C. Turner-Foster, A. L. Gaeta, and M. Lipson, "CMOS-compatible multiple-wavelength oscillator for on-chip optical interconnects," *Nat. Photonics* **4**, 37–40 (2010).
11. L. Razzari, D. Duchesne, M. Ferrera, R. Morandotti, S. Chu, B. Little, and D. Moss, "CMOS-compatible integrated optical hyper-parametric oscillator," *Nat. Photonics* **4**, 41–45 (2010).
12. T. Herr, K. Hartinger, J. Riemensberger, C. Wang, E. Gavartin, R. Holzwarth, M. Gorodetsky, and T. Kippenberg, "Universal formation dynamics and noise of Kerr-frequency combs in microresonators," *Nat. Photonics* **6**, 480–487 (2012).
13. P.-H. Wang, F. Ferdous, H. Miao, J. Wang, D. E. Leaird, K. Srinivasan, L. Chen, V. Aksyuk, and A. M. Weiner, "Observation of correlation between route to formation, coherence, noise, and communication performance of Kerr combs," *Opt. Express* **20**, 29284–29295 (2012).
14. B. Hausmann, I. Bulu, V. Venkataraman, P. Deotare, and M. Lončar, "Diamond nonlinear photonics," *Nat. Photonics* **8**, 369–374 (2014).
15. J. Li, H. Lee, T. Chen, and K. J. Vahala, "Low-pump-power, low-phase-noise, and microwave to millimeter-wave repetition rate operation in microcombs," *Phys. Rev. Lett.* **109**, 233901 (2012).
16. A. Coillet and Y. Chembo, "On the robustness of phase locking in Kerr optical frequency combs," *Opt. Lett.* **39**, 1529–1532 (2014).
17. M. Erkintalo and S. Coen, "Coherence properties of Kerr frequency combs," *Opt. Lett.* **39**, 283–286 (2014).

18. C. Godey, I. V. Balakireva, A. Coillet, and Y. K. Chembo, "Stability analysis of the spatiotemporal Lugiato-Lefever model for Kerr optical frequency combs in the anomalous and normal dispersion regimes," *Phys. Rev. A* **89**, 063814 (2014).
19. S. B. Papp, P. Del'Haye, and S. A. Diddams, "Parametric seeding of a microresonator optical frequency comb," *Opt. Express* **21**, 17615–17624 (2013).
20. Y. K. Chembo and C. R. Menyuk, "Spatiotemporal Lugiato-Lefever formalism for Kerr-comb generation in whispering-gallery-mode resonators," *Phys. Rev. A* **87**, 053852 (2013).
21. S. Coen, H. G. Randle, T. Sylvestre, and M. Erkintalo, "Modeling of octave-spanning Kerr frequency combs using a generalized mean-field Lugiato-Lefever model," *Opt. Lett.* **38**, 37–39 (2013).
22. A. Coillet, I. Balakireva, R. Henriët, K. Saleh, L. Larger, J. Dudley, C. Menyuk, and Y. Chembo, "Azimuthal Turing patterns, bright and dark cavity solitons in Kerr combs generated with whispering-gallery-mode resonators," *IEEE Photon. J.* **5**, 6100409 (2013).
23. P. Del'Haye, K. Beha, S. B. Papp, and S. A. Diddams, "Self-injection locking and phase-locked states in microresonator-based optical frequency combs," *Phys. Rev. Lett.* **112**, 043905 (2014).
24. G. Lin, S. Diallo, R. Henriët, M. Jacquot, and Y. K. Chembo, "Barium fluoride whispering-gallery mode disk-resonator with one billion quality-factor," *Opt. Lett.* **39**, 1–4 (2014).
25. F. Orucevic, V. Lefèvre-Seguin, and J. Hare, "Transmittance and near field characterization of sub-wavelength tapered optical fibers," *Opt. Express* **15**, 13624–13629 (2007).
26. G. Lin, B. Qian, F. Oručević, Y. Candela, J.-B. Jager, Z. Cai, V. Lefèvre-Seguin, and J. Hare, "Excitation mapping of whispering gallery modes in silica microcavities," *Opt. Lett.* **35**, 583–585 (2010).
27. W. Liang, V. Ilchenko, A. Savchenkov, A. Matsko, D. Seidel, and L. Maleki, "Whispering-gallery-mode-resonator-based ultranarrow linewidth external-cavity semiconductor laser," *Opt. Lett.* **35**, 2822–2824 (2010).
28. G. Lin, Y. Candela, O. Tillement, Z. Cai, V. Lefèvre-Seguin, and J. Hare, "Thermal bistability-based method for real-time optimization of ultralow-threshold whispering gallery mode microlasers," *Opt. Lett.* **37**, 5193–5195 (2012).
29. J. Li, H. Lee, K. Y. Yang, and K. J. Vahala, "Sideband spectroscopy and dispersion measurement in microcavities," *Opt. Express* **20**, 26337–26344 (2012).
30. A. A. Savchenkov, A. B. Matsko, W. Liang, V. S. Ilchenko, D. Seidel, and L. Maleki, "Kerr frequency comb generation in overmoded resonators," *Opt. Express* **20**, 27290–27298 (2012).
31. S. Ramelow, A. Farsi, S. Clemmen, J. S. Levy, A. R. Johnson, Y. Okawachi, M. R. E. Lamont, M. Lipson, and A. L. Gaeta, "Strong polarization mode coupling in microresonators," *Opt. Lett.* **39**, 5134–5137 (2014).
32. Y. Liu, Y. Xuan, X. Xue, P.-H. Wang, S. Chen, A. J. Metcalf, J. Wang, D. E. Leaird, M. Qi, and A. M. Weiner, "Investigation of mode coupling in normal-dispersion silicon nitride microresonators for Kerr frequency comb generation," *Optica* **1**, 137–144 (2014).
33. D. V. Strekalov and N. Yu, "Generation of optical combs in a whispering gallery mode resonator from a bichromatic pump," *Phys. Rev. A* **79**, 041805 (2009).
34. T. Hansson and S. Wabnitz, "Bichromatically pumped microresonator frequency combs," *Phys. Rev. A* **90**, 013811 (2014).